Magnetism and Colossal Magnetoresistance of the Pseudo-Ternary Rare-Earth Transition-Metal Compounds, $Eu_{14-x}Ca_xMnSb_{11}$ ($x < 3$)

Hyungrak Kim,[†] Julia Y. Chan,[‡] Marilyn M. Olmstead,[†] Peter Klavins,[§] David J. Webb,[§] and Susan M. Kauzlarich*[,†]

Department of Chemistry, University of California, One Shields Ave., Davis, California 95616, Department of Chemistry, Louisiana State University, Baton Rouge, Los Angeles 70803, and Department of Physics, University of California, One Shields Ave., Davis, California 95616

Received May 23, 2001. Revised Manuscript Received October 10, 2001

The compounds, $Eu_{14-x}Ca_xMnSb_{11}$ ($x < 3$), have been prepared by heating the mixture of stoichiometric amounts of the elements, sealed in a quartz-jacketed Ta tube, in a two-zone furnace with $T_{high} = 1100$ and $T_{low} = 1050$ °C for 10 days. These compounds are isostructural with the Zintl compound $Ca_{14}AlSb_{11}$. The rare-earth transition-metal compounds crystallize in the tetragonal space group $I4_1/acd$, $Z = 8$, $T = 90$ K, $a = 17.2235(7)$ and $c = 22.6555(9)$ Å, $V = 6720.7(5)$ Å^3, and R_1/wR_2 (0.0413/0.1129) for $x = 1.45$ and $a = 17.1737(7)$ and $c = 22.5741(10)$ Å, $V = 6657.9(5)$ Å^3, and R_1/wR_2 (0.0392/0.1122) for $x = 2.83$. Temperature-dependent magnetic susceptibility measurement of the powder samples reveals complex magnetic interactions in the compounds and indicates a canted ferromagnetic configuration for $Eu_{14-x}Ca_xMnSb_{11}$. As the amount of nonmagnetic Ca increases to $x = 2$, the effective magnetic moment decreases from 29.9 to 27.9 μ_B/f.u., and the paramagnetic Curie temperature of the compound increases from 82.4 to 86.4 K at 1000 Oe. The magnetotransport properties of one compound, $Eu_{13}CaMnSb_{11}$ ($x = 1$), were measured and show a close relation to its magnetic properties, especially in the low-temperature region. The influence of chemical substitution on the structural and physical properties of $Eu_{14-x}Ca_xMnSb_{11}$ will be discussed in terms of the site preferences of Ca doping into the four different Eu sites.

Introduction

In the last few decades, there have been a large number of investigations[1−4] on the magnetic properties of ternary rare-earth transition-metal compounds. This is because of the technical application of their huge magnetic anisotropy, which is important for permanent magnetic materials, as well as their intriguing magnetic properties which arise from the combination of itinerant transition-metal magnetism with the localized and anisotropic magnetism of the rare-earth ions. In the case of ternary RTX systems (R = rare earths, T = 3d transition metals Mn, Fe, Co, and Ni, and X = main group 13−15 elements), the magnetic interactions are comprised of three different types: the R−R interaction (4f−4f), the R−T interaction (4f−3d), and the T−T interaction (3d−3d). Many interesting magnetization processes of the RTX compounds have been explained on the basis of the relative strength of the three different exchange interactions and the variation of the mutual orientation of their magnetic sublattices.

The understanding of the 4f−3d exchange interaction is of special importance since it is closely connected to the magnetocrystalline anisotropy of the RTX compound and the interaction parameter J_{RT} changes its sign depending on the type of rare-earth element. A variety of theoretical descriptions[5−7] and experimental approaches[8−12] have been made to investigate this indirect 4f−3d coupling. It is proposed to arise via intra-atomic (R) ferromagnetic 4f−5d exchange interaction and subsequently interatomic (R−T) 5d−3d interaction. However, the study of the magnetic properties of the RTX compounds is far from complete even with the large number of available ternary phases with different compositions and crystal structures.

* To whom correspondence should be addressed.
[†] Department of Chemistry, University of California.
[‡] Louisiana State University.
[§] Department of Physics, University of California.

(1) Buschow, K. H. J. In *Ferromagnetic Materials*; Wohlfarth, E. P., Ed.; North-Holland Publishing Company: Amsterdam, 1980; Vol. 1, pp 297−414.
(2) Li, H. S.; Coey, J. M. D. In *Handbook of Magnetic Materials*; Buschow, K. H. J., Ed.; Elsevier Science Publishers B. V.: Amsterdam, 1991; Vol. 6, pp 1−83.
(3) Szytula, A. In *Handbook of Magnetic Materials*; Buschow, K. H. J., Ed.; Elsevier Science Publishers B. V.: Amsterdam, 1991; Vol. 6, pp 85−180.
(4) Wallace, W. E. *Rare Earth Intermetallics*; Academic Press: New York and London, 1973.
(5) Brooks, M. S. S.; Johansson, B. In *Handbook of Magnetic Materials*; Buschow, K. H. J., Ed.; Elsevier Science Publishers B. V.: Amsterdam, 1993; Vol. 7, pp 139−230.
(6) Richter, M. *J. Phys. D: Appl. Phys.* **1998**, *31*, 1017−1048.
(7) Campbell, I. A. *J. Phys. F: Met. Phys.* **1972**, *2*, L47.
(8) Franse, J. J. M.; Radwanski, J. R. In *Handbook of Magnetic Materials*; Buschow, K. H. J., Ed.; Elsevier Science Publishers B. V.: Amsterdam, 1993; Vol. 7, pp 307−501.
(9) de Boer, F. R.; Zhao, G. Z. *Physica B* **1995**, *211*, 81−86.
(10) de Boer, F. R. *J. Magn. Magn. Mater.* **1996**, *159*, 64−70.
(11) Shimizu, K.; Ichnose, K.; Fukuda, Y.; Shimotomai, M. *Solid State Commun.* **1995**, *96*, 671−674.
(12) Zvezdin, A. K. In *Handbook of Magnetic Materials*; Buschow, K. H. J., Ed.; Elsevier Science Publishers B. V.: Amsterdam, 1995; Vol. 9, pp 405−543.

10.1021/cm010512s CCC: $22.00
Published on Web 12/20/2001

The recently discovered $Eu_{14}MnSb_{11}$ compound[13] is an unique example of this RTX family since experimental data on the coupling between Eu(4f)−Mn(3d) are relatively few and the rare-earth rich RTX phase is not well studied. The crystal structure of the compound can be understood by utilizing the well-known *Zintl-Klemn* concept.[14,15] It is semiconducting at room temperature, as is typical for Zintl phases.[16] The $Eu_{14}MnSb_{11}$ compound provides an opportunity to investigate the R−T exchange interaction because of available experimental data on the isostructural T and R systems. From the study of the alkaline earth analogues of the compound $A_{14}MnSb_{11}$ (A = Ca, Sr, Ba),[17] it was clearly shown that the RKKY-type (Ruderman−Kittel−Kasuya−Yosida) description could be used to describe the T−T magnetic interaction between the Mn's. For the R−R only system, low-temperature antiferromagnetic behavior attributed to R−R interaction has been observed for the isostructural compound $Eu_{14}InSb_{11}$.[18] The complicated magnetization processes and the relatively high transition temperature observed for the $Eu_{14}MnSb_{11}$ RTX system are not well understood due to the complex magnetic interaction between four crystallographically different $4f^7$ Eu(II) magnetic ions and the high-spin $3d^4$ Mn(III) transition-metal ion.

As a systematic approach to probe the R−T magnetic interaction, the synthesis and characterization of the physical properties of the $Eu_{14-x}Ca_xMnSb_{11}$ ($x < 3$) compounds are reported in this paper. The idea of nonmagnetic ion substitution into magnetic Eu sites for the detailed magnetic study has been reported for other compounds.[19−22] A small amount of Ca has been substituted into the Eu sites of $Eu_{14}MnSb_{11}$ to probe the magnetic exchange interactions of the compound. The Ca substitution was also motivated by the effort to investigate the colossal magnetoresistance (CMR) behavior of the compound. This paper presents the crystal structure change and site preferences of the Ca dopant of the $Eu_{14-x}Ca_xMnSb_{11}$ (nominal compositions, $x = 1$ and 2) solid solution system. The effect of decreasing concentration of the rare-earth element on magnetism and MR is discussed on the basis of the three different types (R−R, R−T, and T−T) of magnetic exchange interactions.

Experimental Section

Synthesis. Eu metal was obtained (Ames Lab, 99.999%) and cut into small pieces. Ca pieces (J. Matthey, 99.99%) and Sb (J. Matthey, 99.9999%) were used as received. Mn flakes (J. Matthey, 99.98%) were first cleaned in a 5% HNO_3/CH_3OH solution, transferred into a drybox, and ground into a powder. All materials were handled in an argon drybox. Both of the $Eu_{14-x}Ca_xMnSb_{11}$ samples (nominally $x = 1$, 2) were prepared by weighing stoichiometric amounts of the elements in a drybox, loading into a clean tantalum tube with a sealed end, and subsequently sealing with an argon-filled arc welder. Ta tubes had been cleaned prior to arc welding with 20% HF, 25% HNO_3, and 55% H_2SO_4 solution. The sealed Ta tube was further sealed in a fused silica tube under $^1/_5$ atm purified argon. Reflective polycrystalline pieces and single-crystal needles (1−2 mm) were obtained by heating the mixtures in a two-zone furnace with $T_{high} = 1100$ and $T_{low} = 1050$ °C for 10 days, followed by furnace cooling. All reactions were opened and examined in a nitrogen-filled drybox equipped with a microscope with water levels less than 1 ppm.

Table 1. Data Collection Parameters and Crystallographic Data

compound	$Eu_{13}CaMnSb_{11}$	$Eu_{12}Ca_2MnSb_{11}$
crystal dimension, mm^3	0.05 × 0.06 × 0.09	0.05 × 0.05 × 0.15
color and habit	metallic needle	metallic needle
crystal system	tetragonal	tetragonal
space group, Z	$I4_1/acd$, 8	$I4_1/acd$, 8
temperature, K	90	90
a, Å	17.2235(7)	17.1737(7)
c, Å	22.6555(9)	22.5741(10)
V, $Å^3$	6720.7(5)	6657.9(5)
ρ_{cal}, mg m^{-3}	6.74	6.58
θ_{max}, deg	31.53	31.51
μ Mo Kα, mm^{-1}	33.012	31.628
scan range (omega), ω	0.3	0.3
acquisition time, sec	30	30
no. collected reflns	30 806	30 578
no. unique reflns	2802	2761
no. reflns with $I > 2\sigma(I)$	2371	2322
no. params refined	50	50
R_1[a] for $[F^2 > 2\sigma(F^2)]$	0.0413	0.0392
wR_2[b]	0.1129	0.1122
$(\Delta\rho)_{max}$, $(\Delta\rho)_{min}$ (e A^{-3})	7.830, −6.257	7.266, −5.367

[a] $R_1 = \sum||F_o| - |F_d||/\sum|F_o|$. [b] $wR_2 = \sum[w(F_o^2 - F_c^2)^2]/\sum[w(F_o^2)^2]]^{1/2}$.

Structure Determination. The tantalum tube was opened in a drybox equipped with a microscope. Metallic and highly reflective needle crystals (1−2 mm) were transferred to Exxon Paratone N oil for X-ray structure determination. A suitable crystal (0.05 × 0.06 × 0.09 mm^3 for $Eu_{13}CaMnSb_{11}$ and 0.05 × 0.05 × 0.15 mm^3 for $Eu_{12}Ca_2MnSb_{11}$) was mounted on a thin glass fiber and positioned under a 90 K cold stream of N_2 in a Bruker SMART 1000 CCD diffractometer equipped with a CRYO COOLER low-temperature apparatus (CRYO INDUSTRIES of America, Inc.). No decomposition of the crystal was observed during data collection (inferred from the intensity of reflections collected on 50 redundant frames at the beginning and end of data collection). The SMART software[23] was used for data collection, and SAINT[24] was used for data integration. The absorption correction was performed by using SADABS.[23] The structure was solved by direct methods and refined using SHELXL-97.[25] Data collection parameters and crystallographic data are provided in Table 1. Detailed crystallographic data and anisotropic thermal parameters are provided as Supporting Information. X-ray powder diffraction data of the products were obtained by using an Enraf-Nonius Guinier camera equipped with a quartz monochromator to produce Cu $K\alpha_1$ radiation. Powdered silicon (NBS, #640b) was included in the samples as an internal standard.

Magnetic Susceptibility and Transport Measurements. DC magnetization data were obtained with a Quantum

(13) Rehr, A.; Kauzlarich, S. M. *J. Alloys Compd.* **1994**, *207/208*, 424−426.
(14) Zintl, E. *Angew. Chem.* **1939**, *52*, 1.
(15) Klemm, W. *Proc. Chem. Soc., London* **1958**, 329.
(16) Miller, G. J. In *Chemistry, Structure, and Bonding of Zintl Phases and Ions*; Kauzlarich, S. M., Ed.; VCH Publishers: New York, 1996; pp 245−274.
(17) Rehr, A.; Kuromoto, T. Y.; Kauzlarich, S. M.; Castillo, J. D.; Webb, D. J. *Chem. Mater.* **1994**, *6*, 93−99.
(18) Chan, J. Y.; Wang, M. E.; Rehr, A.; Kauzlarich, S. M.; Webb, D. J. *Chem. Mater.* **1997**, *9*, 2132−2138.
(19) Tadokoro, Y.; Shan, Y. J.; Nakamura, T.; Nakamura, S. *Solid State Ionics* **1998**, *108*, 261−267.
(20) Majumdar, S.; Mallick, R.; Sampathkumaran, E. V.; Paulose, P. L.; Gopalakrishinan, K. V. *Phys. Rev. B* **1999**, *59*, 4244−4248.
(21) Abramovich, A.; Demin, R.; Koroleva, L.; Michurin, A.; Maslov, K. A.; Mukovskii, Ya. M. *Phys. Lett. A* **1999**, *259*, 57−61.
(22) Vonlanthen, P.; Felder, E.; Wallti, Ch.; Paschen, S.; Ott, H. R.; Young, D. P.; Bianchi, A. D.; Fisk, Z. *Physica B* **2000**, *284−288*, 1361−1362.
(23) *SMART*; Siemens Analytical X-ray Systems, Inc.: Madison, WI, 1994.
(24) *SAINT*, 6th ed.; Siemens Analytical X-ray Systems, Inc.: Madison, WI, 1999.
(25) Sheldrick, G. M. *SHELXTL*, 5.10; Bruker AXS Inc.: Madison, WI, 1997.

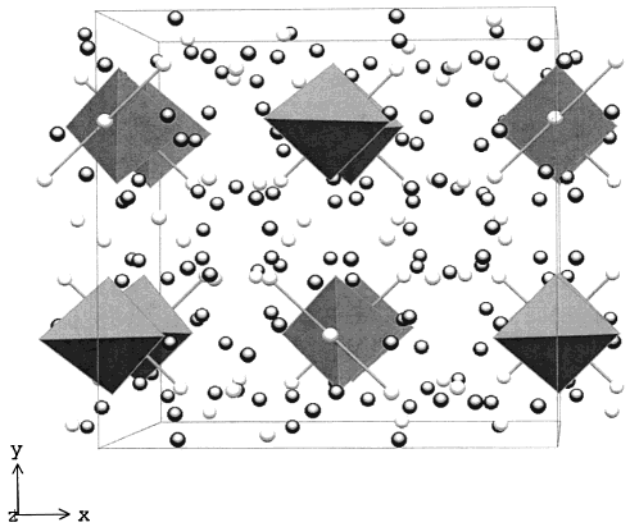

Figure 1. Perspective view down the *z*-axis of the unit cell of $Eu_{14}MnSb_{11}$: gray polyhedra, $MnSb_4$; black circles, Eu; white, Sb.

Design MPMS Superconducting Quantum Interference Device (SQUID) magnetometer with a 7 T superconducting magnet. The data were collected with the Magnetic Property Measurement System (MPMS) software[26] supplied by Quantum Design. For single-crystal magnetic measurements, the same crystal that was used for the structure determination was placed in a low background sample holder. Powdered samples were prepared in a drybox, by loading 30−50 mg into a gelatin capsule, and suspended in a low background sample holder. MR measurement of the $Eu_{13}CaMnSb_{11}$ compound was performed on a needle-shaped single crystal with dimensions of $0.05 \times 0.06 \times 1$ mm^3 by using a standard four-probe method. A constant current (1mA) was applied to the sample along the crystal *c*-axis through the two outer leads (Keithley model 224 current source), and the voltage was measured across the two inner leads (Keithley model 196 nanovoltmeter).

Results and Discussion

Structure. The crystal structures of the mixed system were first refined as $Eu_{14}MnSb_{11}$, and then Ca was substituted into the various Eu sites. Various models were employed, i.e., sequential substitution of Ca into the different Eu sites, while the thermal parameters were kept equal. The model presented in this paper provides the lowest *R*'s and reasonable thermal parameters in the refinements. All $Eu_{14-x}Ca_x$-$MnSb_{11}$ ($x = 0-3$) compounds are isostructural to Ca_{14}-$AlSb_{11}$[27], and this structure type has been described in detail previously.[13,17,27−29] Figure 1 shows a perspective view of the unit cell along the *c*-axis of $Eu_{14}MnSb_{11}$. In brief, $Eu_{14}MnSb_{11}$ crystallizes in a body-centered tetragonal unit cell in the space group $I4_1/acd$ with 8 formula units (208 atoms). A formula unit consists of 14 interstitial Eu^{2+}, 4 isolated Sb^{3-}, a distorted $MnSb_4^{9-}$ tetrahedron, and a Sb_3^{7-} linear anion. The structure is characterized by alternating tetrahedra and linear Sb_3^{7-} anions. There are four crystallographically inequivalent sites of Eu and Sb. All the Mn sites in the crystal structure are equivalent and approximately 10 Å apart from their nearest neighbors.

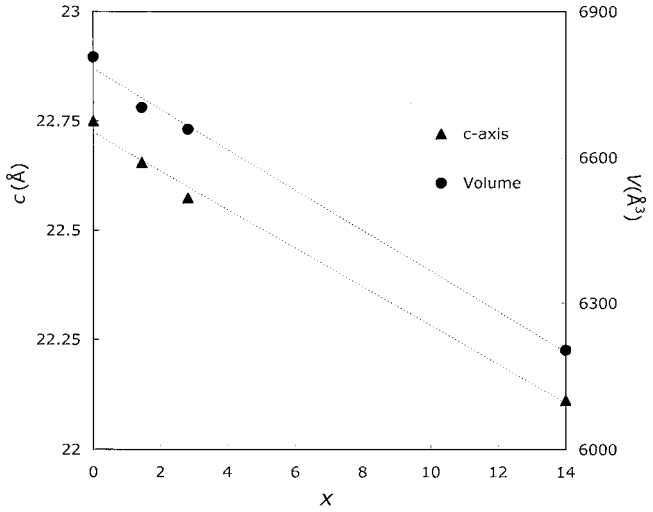

Figure 2. Lattice parameter changes as a function of Ca doping amount in $Eu_{14-x}Ca_xMnSb_{11}$ single crystals.

The lattice parameters of the $Eu_{14-x}Ca_xMnSb_{11}$ compounds decrease with increasing *x*, as shown in Table 1 and Figure 2. The linear decrease of the lattice parameters is consistent with Vegard's rule and indicates that this system should be a solid solution. The systematic decrease of the lattice parameters with increase in the amount of Ca substitution for Eu is attributed to the smaller ionic radius of Ca^{2+} (1.14 Å) compared to that of Eu^{2+} (1.31 Å).[30] The cation size influence on the lengths of the *a-axis* and *c*-axis is mediated by changes of the cation−Sb and cation−cation distances. Table 2 presents selected bond distances for $Eu_{14-x}Ca_xMnSb_{11}$ ($x = 1, 2$). The decrease of the average bond distance of Eu−Sb by Ca substitution ranges from 0.4 to 1.0% and in the case of Eu−Eu, ranges from 0.7 to 0.8%. The bonds which do not contain Eu show much less dependence on doping, from 0.1 (Mn−Sb(2)) to 0.3% (Sb(1)−Sb(4)). The most distinct change is seen in the Eu(4)−Sb(3) distance which is 3.8560(7) Å for $x = 0$ and 3.7953(8) Å for $x = 2$: a change of 1.6%. A similar cation size effect was observed in the study of $A_{14}MnPn_{11}$ (A = alkaline earths, Pn = main group 15 elements, As, Sb, Bi) analogues.[31] The A_{14}-$MnPn_{11}$ compounds show a linear decrease in the A−Pn distances and Mn−Mn distances as the size of the ionic radius of the alkaline earth element decreases.

A salient feature of the Ca substitution into the Eu sites is the manner by which the Ca atoms are distributed throughout the four different unique crystallographic sites. The Ca atoms preferentially occupy the Eu(3) site first and, subsequently, occupy the other sites in the order Eu(1), Eu(4), and Eu(2), as shown in Table 3. It is remarkable that the Ca replacement on the Eu(3) site becomes as high as 40% with only 14% Ca doping overall ($x = 2$ in $Eu_{14-x}Ca_xMnSb_{11}$). Figure 3 shows the trend of Ca preference for $x < 3$. Due to the divalency of both Eu and Ca, the preferences of the two different elements for specific sites cannot be attributed to the

(26) *MPMS XL7*; Quantum Design Inc.: San Diego, CA 92121.
(27) Cordier, G.; Schäfer, H.; Stelter, M. *Z. Anorg. Allg. Chem.* **1984**, *519*, 183−188.
(28) Kuromoto, T. Y.; Kauzlarich, S. M.; Webb, D. J. *Chem. Mater.* **1992**, *4*, 435−440.
(29) Kauzlarich, S. M. In *Chemistry, Structure, and Bonding of Zintl Phases and Ions*; Kauzlarich, S. M., Ed.; VCH Publishers: New York, 1996; pp 245−274.
(30) Shannon, R. D. *Acta Crystallogr.* **1976**, *A32*, 751.
(31) Brook, S. L.; Weston, L. J.; Olmstead, M. M.; Kauzlarich, S. M. *J. Solid State Chem.* **1993**, *107*, 513−523.

Table 2. Selected Bond Distances (Å) and Angles (deg)

	$Eu_{14}MnSb_{11}$	$Eu_{13}CaMnSb_{11}$	$Eu_{12}Ca_2MnSb_{11}$
Sb(1)−Sb(4)	3.2624(7)	3.2548(9)	3.2519(8)
Sb(1)−Eu(1) × 2	3.3241(5)	3.3125(7)	3.3045(7)
Sb(1)−Eu(2) × 2	3.4241(5)	3.4133(6)	3.4084(6)
Sb(1)−Eu(3)	3.4910(3)	3.4738(4)	3.4594(4)
Sb(1)−Eu(4)	3.3316(7)	3.3148(8)	3.3018(8)
Sb(2)−Mn × 4	2.7895(5)	2.7854(6)	2.7856(6)
Sb(2)−Eu(1)	3.3158(6)	3.2940(8)	3.2771(8)
Sb(2)−Eu(1′)	3.3550(7)	3.3380(8)	3.3215(9)
Sb(2)−Eu(2)	3.2583(7)	3.2478(8)	3.2430(8)
Sb(2)−Eu(2′)	3.8381(7)	3.8330(8)	3.8306(8)
Sb(2)−Eu(3)	3.3967(6)	3.3773(9)	3.3612(9)
Sb(2)−Eu(4)	3.2842(7)	3.2740(8)	3.2665(8)
Sb(2)−Eu(4′)	3.5088(7)	3.4978(9)	3.4908(8)
Sb(3)−Eu(1)	3.3040(7)	3.2857(9)	3.2724(9)
Sb(3)−Eu(1′)	3.3359(6)	3.3265(8)	3.3193(9)
Sb(3)−Eu(2)	3.3116(7)	3.3024(8)	3.2945(8)
Sb(3)−Eu(2′)	3.4015(7)	3.3905(8)	3.3822(8)
Sb(3)−Eu(3)	3.2521(7)	3.2321(9)	3.2198(9)
Sb(3)−Eu(4)	3.3073(7)	3.2914(8)	3.2775(8)
Sb(3)−Eu(4′)	3.3296(7)	3.3107(8)	3.2970(8)
Sb(3)−Eu(4″)	3.8560(7)	3.8209(9)	3.7953(8)
Sb(4)−Eu(1) × 4	3.3283(4)	3.3145(5)	3.3030(6)
Sb(4)−Eu(2) × 4	3.5785(4)	3.5673(5)	3.5612(5)
Mn−Eu(2) × 4	3.6188(4)	3.6047(5)	3.5914(5)
Sb(2)−Mn−Sb(2′)	105.23(1)	105.15(1)	105.04(1)
Sb(2)−Mn−Sb(2″)	118.34(2)	118.51(3)	118.75(3)
Mn···Mn	10.3512(8)	10.3073(6)	10.2753(8)

Table 3. Fractional Site Occupancies (%) of Ca in Four Crystallographic Unique Eu Sites

	$Eu_{14}MnSb_{11}$	$Eu_{13}CaMnSb_{11}$	$Eu_{12}Ca_2MnSb_{11}$
x^a	0	1.45(4)	2.83(4)
Eu(1)	100	85.8(3)	72.0(3)
Ca(1)	0	14.2(3)	28.0(3)
Eu(2)	100	95.5(3)	92.5(3)
Ca(2)	0	4.5(3)	7.5(3)
Eu(3)	100	78.8(4)	60.0(4)
Ca(3)	0	21.2(4)	40.0(4)
Eu(4)	100	92.5(3)	85.2(3)
Ca(4)	0	7.5(3)	14.8(3)

[a] x in $Eu_{14-x}Ca_xMnSb_{11}$ by crystal structure refinement.

differences in charge or valence electron concentration of the atomic sites, which have been used to understand fractional occupancies of different valence elements from site to site in the various other structures.[32,33]

From a structural point of view, a plausible explanation of the site preference of Ca can be proposed. Figure 4 shows the four pseudo-octahedral Eu sites surrounded by six Sb's. The Eu(3) site is highly symmetric when it is compared to the other three. It also has the shortest Eu−Sb bond distance (Eu(3)−Sb(3), 3.252 Å) and average Eu−Eu distance (3.919 vs 4.185−4.266 Å for the other three). Thus, the preference for Ca to substitute first in the Eu(3) site may originate from the high symmetry of the site. The smaller Ca^{2+} ion would be more appropriate in this restricted site providing less structural perturbation. It is noteworthy that the Eu(3) site has very large displacement parameters and has been the site of defects, for example, in the compounds $Sr_{13}NbAs_{11}$ and $Eu_{13}NbAs_{11}$.[34] In the case of the most distorted Eu(2) site, it has the widest variation of the

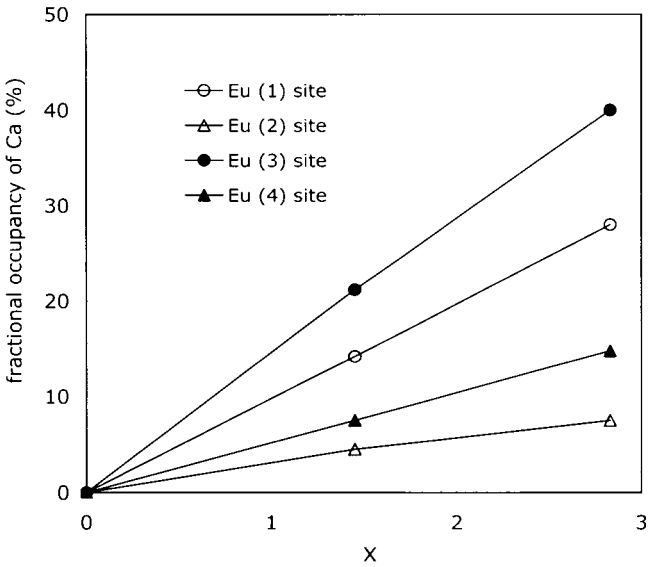

Figure 3. Fractional occupancies of Ca in four different Eu crystallographic sites.

Sb−Eu−Sb angle (55.5−136.8°). The average Eu−Eu distance (4.266 Å) of this site is longer that the other three (3.919−4.223 Å). As a result, the Eu(2) site is more available to the larger metal cation, Eu^{2+}. Ca replacement on the Eu(2) site is just 7.5% when the total doping of Ca is 14% ($x = 2$) as provided in Table 3. It is almost impossible to evaluate the contribution of each Eu site on the magnetization process of the $Eu_{14}MnSb_{11}$ compound. However, by knowing the preferential substitution of the nonmagnetic Ca cations into the magnetic four Eu sites, one may be able to gain a level of understanding of each Eu site contribution. A view showing the relationship of the $MnSb_4$ tetrahedra with the four different Eu sites is presented in Figure 5. Eu(2) and Eu(4) are positioned close to the $MnSb_4$ tetrahedra and are expected to have an influence on the Mn−Mn magnetic interaction. Eu(1) and Eu(3) directly link four $MnSb_4$ tetrahedra to a central $MnSb_4$ tetrahedron.

Magnetism. The magnetic properties of $Eu_{14}MnSb_{11}$[18,35] have been reported and compared to its alkaline earth analogues. $Eu_{14}MnSb_{11}$ has the highest T_C, 92 K, among all the compounds of the $A_{14}MnPn_{11}$ family measured to date. Two magnetic long range ordering temperatures were reported for $Eu_{14}MnSb_{11}$, 92 and 15 K. The 92 and the 15 K transitions have been attributed to a ferromagnetic Mn−Mn RKKY interaction and to an antiferromagnetic Eu−Eu ordering, respectively. However, from this study of temperature-dependent magnetization processes of the $Eu_{14-x}Ca_xMnSb_{11}$ solid solutions, it is clear that the magnetic behavior of the $Eu_{14}MnSb_{11}$ compound is more complex. The $Eu_{14}MnSb_{11}$ compound is better categorized as a ferrimagnetic compound where two or more magnetic sublattices interact with different orientations. The ferrimagnetic behavior is not unexpected, considering the many possible spin orientations from R−R, R−T, and T−T exchange interactions in this ternary rare-earth transition metal compound.

(32) Franzen, H. F.; Kockerling, M. *Prog. Solid State Chem.* **1995**, *23*, 265.
(33) Miller, G. J. *Eur. J. Inorg. Chem.* **1998**, *55*, 523.
(34) Vidyasagar, K.; Hönle, W.; Schnering, H. G. v. *Z. Anorg. Allg. Chem.* **1996**, *622*, 518−524.
(35) Chan, J. Y.; Kauzlarich, S. M.; Klavins, P.; Shelton, R. N.; Webb, D. J. *Chem. Mater.* **1997**, *9*, 3132−3135.

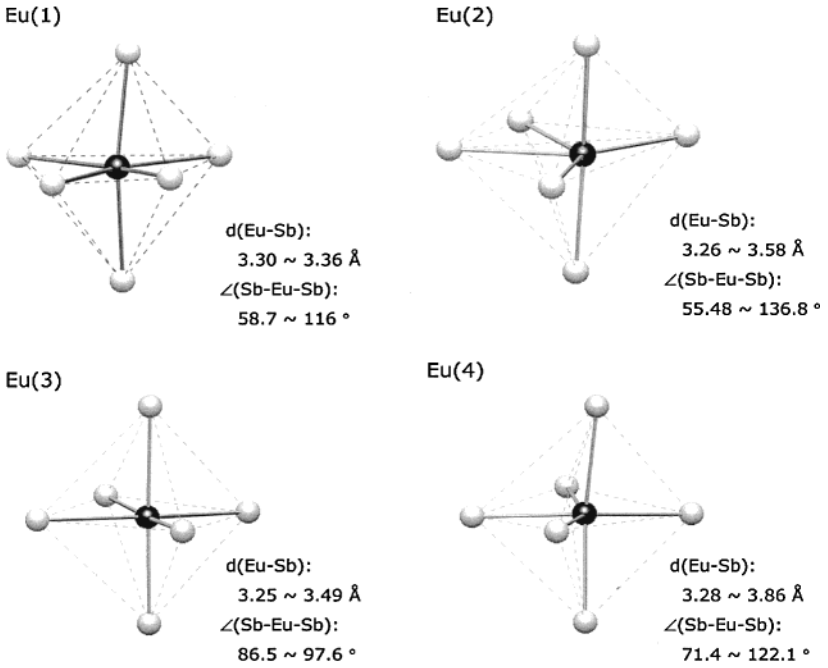

Figure 4. Four different crystallographic Eu sites surrounded by six Sb: black circles, Eu; gray, Sb.

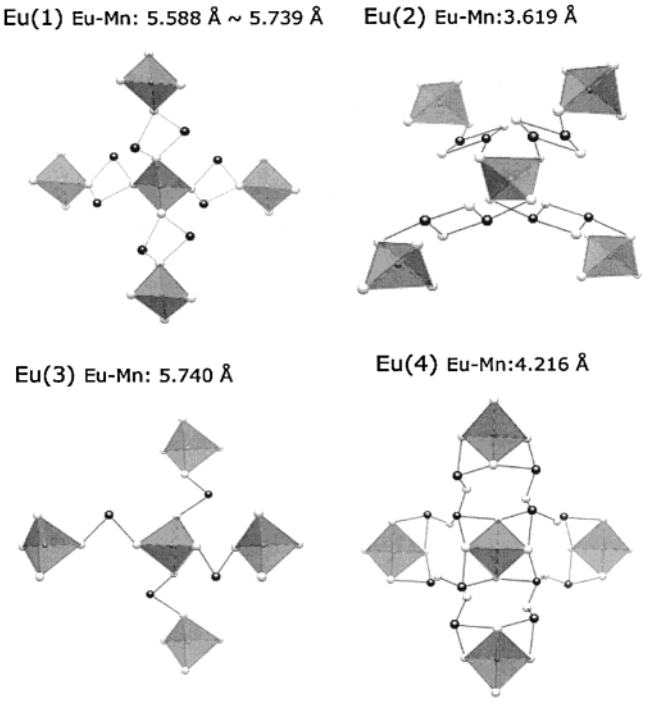

Figure 5. View showing the relationship of the $MnSb_4$ tetrahedra with four Eu. The Mn atoms reside in the center of the gray polyhedra: black circles, Eu; white, Sb.

Figure 6 shows temperature-dependent magnetization of the polycrystalline sample of the $Eu_{14-x}Ca_xMnSb_{11}$ solid solutions, $x = 0$, 1, 2, and 14, in the applied field of 1000 Oe. The two end compounds, i.e., $Eu_{14}MnSb_{11}$ and $Ca_{14}MnSb_{11}$, have been synthesized under the same conditions of the mixed system, and their data have been added for comparison. The magnetization curves in the various low magnetic fields are plotted as a function of temperature in Figure 7. The general feature of the temperature-dependent magnetization of the mixed system is similar to the undoped one, $Eu_{14}MnSb_{11}$, but there are distinct decreases in the magnetic

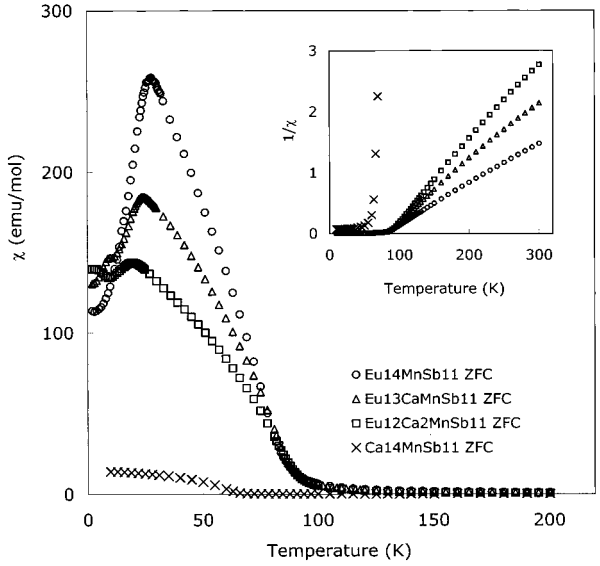

Figure 6. Temperature-dependent magnetization of powder samples of $Eu_{14-x}Ca_xMnSb_{11}$.

moment and shifts in the magnetic ordering temperatures caused by the small amount of Ca substitution. The curvatures in the M vs T data, shown in Figures 6 and 7, indicate that there may be two or more magnetic sublattices involved with their spins oriented in the different directions. A canted ferromagnetic or ferrimagnetic configuration may occur between 3d and 4f sublattices.

The origin of the high transition temperature of $Eu_{14}MnSb_{11}$ compared to the alkaline earth compound is attributed to R−T exchange interactions. There is no doubt that a RKKY-type Mn−Mn exchange interaction triggers the ferromagnetic transition of $Ca_{14}MnSb_{11}$ at 65 K.[17] However, the increase in T_C for the $Eu_{14}MnSb_{11}$ compound must be attributed to both T−T and R−T interactions. In Figure 6, the increased magnitude of magnetic susceptibility of $Eu_{14}MnSb_{11}$ compared to $Ca_{14}MnSb_{11}$ indicates that the Eu magnetic moments are

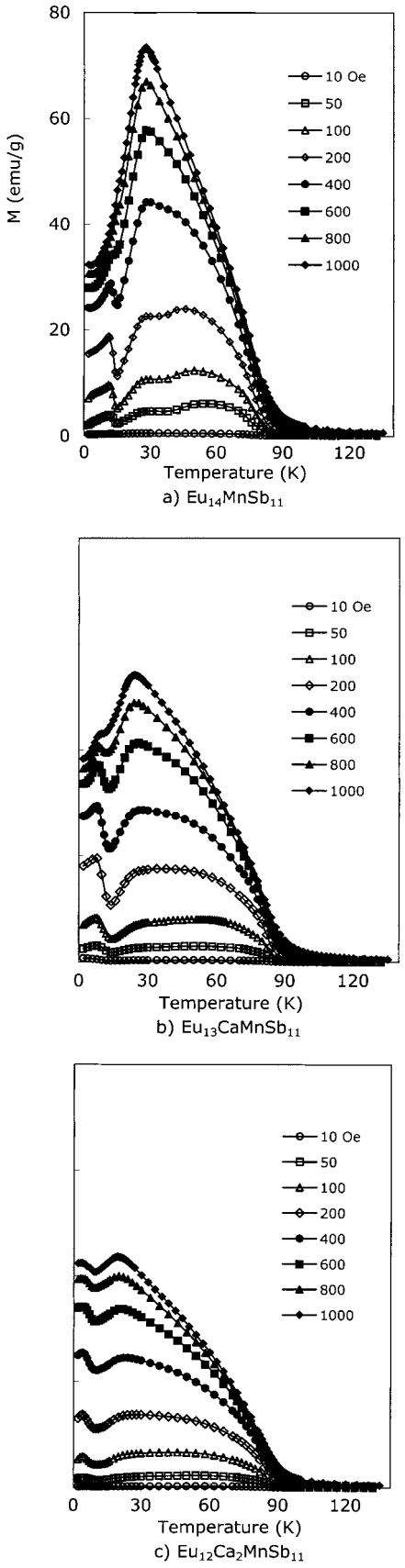

Figure 7. Temperature-dependent magnetization of powder samples of $Eu_{14-x}Ca_xMnSb_{11}$ in the low fields.

also involved in the magnetic ordering at 92 K. The enhanced magnetic interaction between transition metals in $Eu_{14}MnSb_{11}$ is established with the help of surrounding Eu local 4f moments via intra-atomic 5d polarization and subsequently the interatomic Mn(3d)−Eu(5d) exchange interaction.

We exclude here the contribution of the Eu−Eu magnetic interaction to the high-temperature magnetic transition, since R−R interactions are generally very weak in RTX systems. Also, there is no magnetic ordering near the transition temperature in the case of the R−R only analogue of the compound $Eu_{14}InSb_{11}$.[18] The distances of the Eu(2) and Eu(4) sites to Mn (Eu(2)−Mn, 3.619 Å; Eu(4)−Mn, 4.216 Å) are much shorter than the other two (Eu(1)−Mn, 5.588 Å; Eu(2)−Mn, 5.739 Å) as shown in Figure 5. Therefore, from simple spatial considerations, two Eu sites, Eu(2) and Eu(4), may have the largest R−T magnetic interaction. The Eu 4f magnetic sublattice will introduce a magnetocrystalline anisotropy in the compound. There is a significant difference between parallel and perpendicular magnetization measurements of $Eu_{14-x}Ca_xMnSb_{11}$ ($x = 0$, 1) single crystals, as shown in Figure 8. The difference in parallel and perpendicular magnetization may be due to the alignment of the Eu(2) and Eu(4) sites along the *c*-axis.

Table 4 provides results from fits of the high temperature (100−300 K) susceptibility data to a modified Curie−Weiss law. Analysis of the data in the paramagnetic regime illustrates that the effective magnetic moment decreases as nonmagnetic Ca substitution increases. Interestingly, the difference between the experimental magnetic moment and the calculated value for $(14-x)$ Eu^{2+} and 1 Mn^{3+} increases with increasing Ca. A possible reason for the sharp decrease in the moment for the mixed systems could be that some of the Eu are present as Eu^{3+}. If a small amount of Eu^{3+} is induced by Ca substitution, it would change the total magnetic moment of the compound significantly, because of the large difference of the magnetic moments (0 μ_B for Eu^{3+} and 7.94 μ_B for Eu^{2+}). The reduction in moment may also be induced by antiferromagnetic interaction between Eu and Eu and/or Eu and Mn.

The trends of the paramagnetic Curie temperature and ferromagnetic transition temperature from Table 4 also show an unexpected change. In $Eu_{14-x}Ca_xMnSb_{11}$, we observe a slight increase of the paramagnetic Curie temperature as Ca substitution increases up to $x = 2$. The preferential replacement of Ca in the Eu(3) and Eu(1) sites is the main cause of the increase. Either those sites influence the conduction electron polarization, which can change T_C in a RKKY-type magnetic system, or the Eu's on those sites frustrate the rest of the spins, and preferential removal of them allows T_C to increase. It is well-known that frustrating interactions decrease T_C. Thus, the preferential elimination of the rare-earth element for an alkaline earth element increases the transition temperature.

The long-range magnetic ordering at low temperature, below 30 K, is attributed to the onset of antiferromagnetic Eu−Eu ordering.[18] Presumably, all the Eu's are involved in the antiferromagnetic ordering since most Eu−Eu near neighbor distances are less than 4.65 Å, which is smaller than the atomic spacing (4.83 Å) of Eu metal.[36] Metallic Eu is body-centered cubic and orders

(36) Legvold, S. In *Ferromagnetic Materials*; Wohlfarth, E. P., Ed.; North-Holland Publishing Company: Amsterdam, 1980; Vol. 1, pp 297−414.

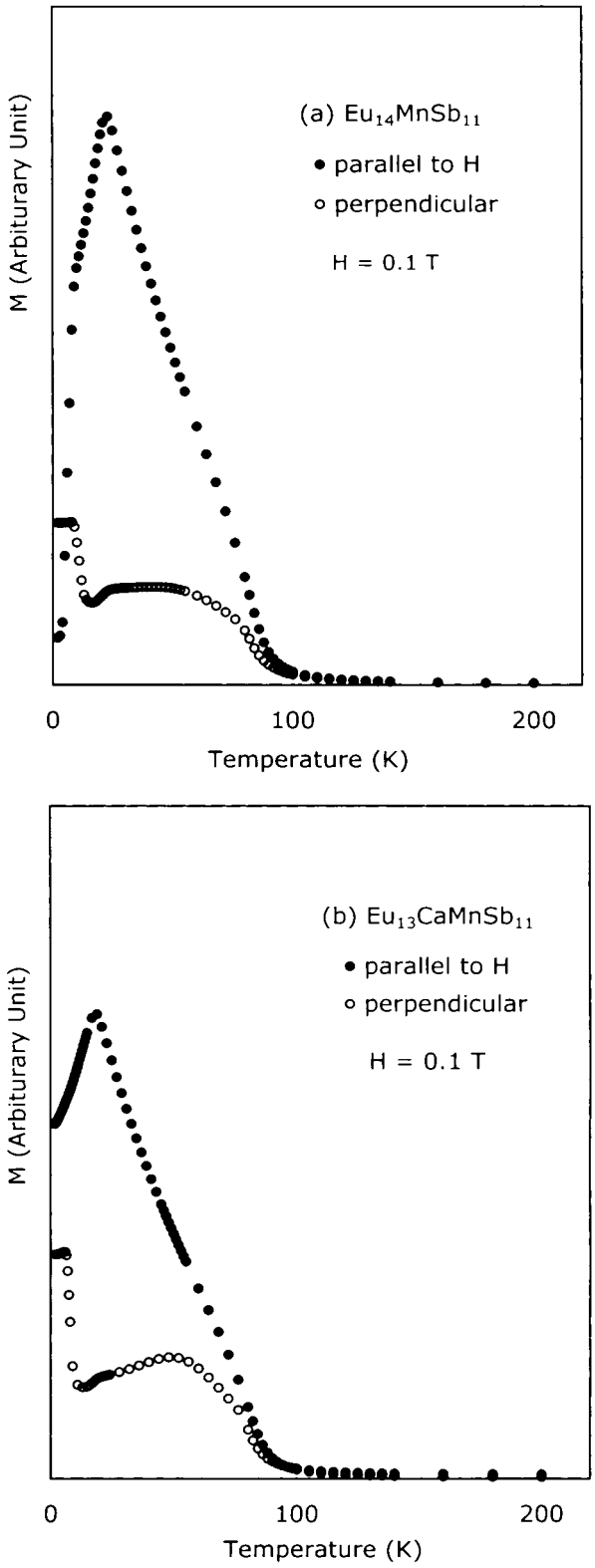

Figure 8. Magnetization of $Eu_{14}MnSb_{11}$ and $Eu_{13}CaMnSb_{11}$ single crystals as a function of temperature.

antiferromagnetically at 90.4 K via the RKKY interaction. This low-temperature R−R ordering will have a strong influence on the spin orientation of the Eu(2) and Eu(4) sites, which causes them to be canted ferromagnetic above the low-temperature transition. Therefore, a new antiferromagnetic R−R sublattice might decrease the total magnetization of the compound below the transition temperature. As Ca substitution increases, the transition temperature decreases from 28.0 K for the undoped $Eu_{14}MnSb_{11}$ sample to 19.5 K for $x = 2$ ($Eu_{12}Ca_2MnSb_{11}$). This low-temperature effect, along with the increase in T_C as Ca substitutes on the Eu(3) and Eu(1) sites, can be attributed to the loss of frustration associated with those sites.

Table 4. Magnetic Properties of $Eu_{14-x}Ca_xMnSb_{11}$ Compounds

	$Eu_{14}MnSb_{11}$	$Eu_{13}CaMnSb_{11}$	$Eu_{12}Ca_2MnSb_{11}$
M_w	3521.698	3409.7	3297.9
χ_o[a] (emu/mol)	0.068(6)	0.0004(1)	−0.015(6)
C[a]	111.6(5)	90.6(7)	71.0(5)
μ_{eff}[b] (μ_B)	29.9(1)	26.9(2)	23.8(2)
μ_{cal}[c] (μ_B)	30.1	29.0	27.9
θ[a] (K)	82.4(1)	84.9(1)	86.4(1)
T_C (K)	91	94	96
T_N (K)	28.0	24.5	19.5
fit range (K)	100−300	100−300	100−300

[a] Obtained from fitting the data to equation $\chi = \chi_o + C/(T-\theta)$. [b] Using the equation $\mu_{eff} = (8C)^{1/2}$. [c] Calculated as such: Eu-Mn compound is $\mu^2 = (14\text{-}x)\mu^2_{Eu} + \mu^2_{Mn}$.

Experimental results of the low field magnetization measurement are also plotted in Figure 7. As the temperature decreases below the R−R ordering temperature, the magnetization curve shows a dip at 15 K and increases slightly after that. It changes slope again around 11 K for $Eu_{14}MnSb_{11}$. The behavior is similar to the compensation point, which has been found in V- or N-type ferrimagnetic materials.[37] In fact, there is a large discrepancy between two different directional measurements of single-crystal samples as shown in Figure 8. When a single crystal is aligned parallel to the magnetic field, it shows a sharp decrease in its magnetization at 15 K. On the contrary, magnetization increases sharply after the transition if the crystal is aligned perpendicular to the magnetic field. Therefore, the transitions at 15 and 11 K for $Eu_{14}MnSb_{11}$ in Figure 7 could be cooperative results of highly magnetocrystalline anisotropic magnetization considering the M vs T plots of single-crystal data in Figure 8. Plots of field-dependent magnetization of polycrystalline samples of the solid solution system are presented in Figure 9 at two different temperatures, 5 and 50 K. At 5 K, the Eu−Eu spins are antiferromagnetically coupled. At 50 K, the sample is below T_C and above the low-temperature magnetic ordering. The saturation moment value of the doped $Eu_{14-x}Ca_xMnSb_{11}$ compound decreases in both temperatures as the amount of Ca replacement increases. All samples show extremely small coercive fields.

Magnetoresistance. Figures 10 and 11 show the temperature-dependent resistivity of a single crystal of $Eu_{13}CaMnSb_{11}$ oriented parallel and perpendicular to H, respectively, at 0−6 T. A transition is observed near 86 K, which is consistent with the paramagnetic Curie temperature of the compound, 85 K, signaling the onset of long-range magnetic ordering similar to $Eu_{14}MnSb_{11}$.[35] These coincident magnetic and electronic transitions are common in the perovskite CMR and pyrochlores.[38] Figure 12 shows a plot of MR ($MR = [(\rho(H) - \rho(0))/\rho(H)] \times 100\%$) as a function of temperature. The MR effects are of a similar order of magnitude as those of

(37) Belov, K. P. *Magnetic Transitions*; Consultants Bureau: New York, 1961.

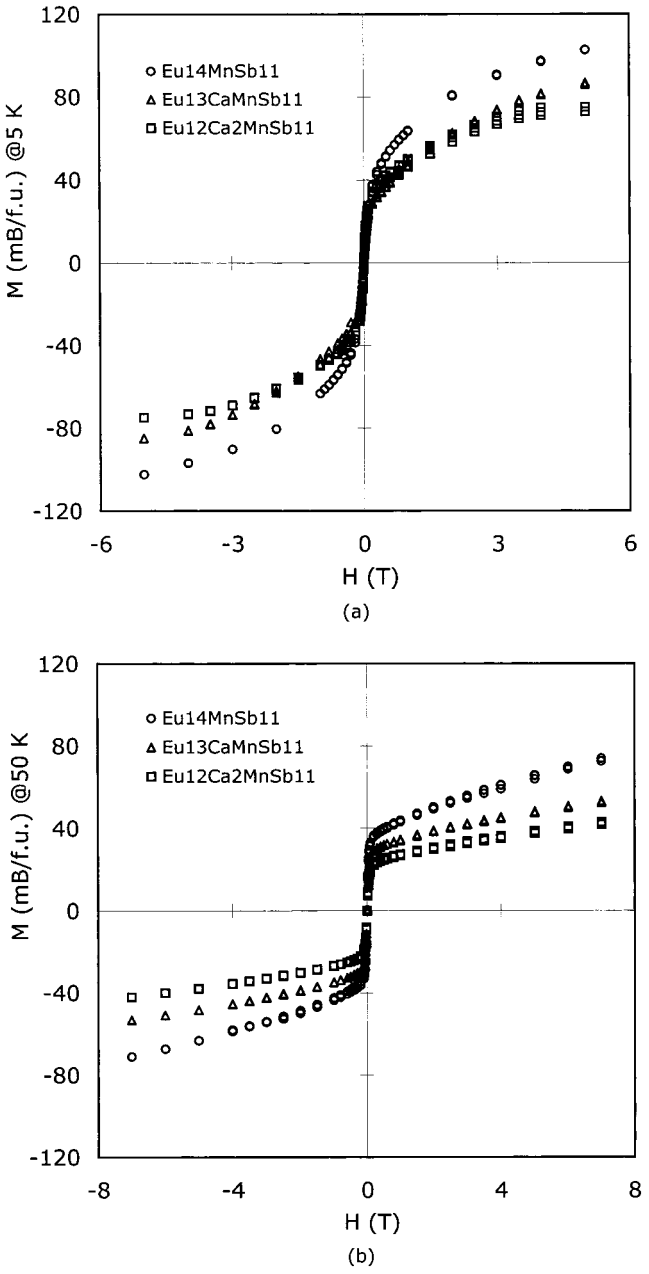

Figure 9. Hysteresis loop of polycrystalline $Eu_{14-x}Ca_xMnSb_{11}$ measured at two temperatures: (a) 5 K; (b) 50 K.

$Eu_{14}MnSb_{11}$. A large negative MR is observed for $Eu_{13}CaMnSb_{11}$ beginning at 150 K and shows its pronounced effect (ca. −32%) around 80 K at 6 T. Above the transition, the suppression of resistivity by the magnetic field diminishes as temperature increases. Interestingly, the MR effect reaches its maximum (ca. −80%) at the lowest temperature, 2 K at 6 T, and not near its first long range ordering temperature, 86 K. The same behavior has been observed in $Eu_{13.97}Gd_{0.3}MnSb_{11}$,[39] but the origin of the sharp increase below 6 K is not well understood.

The CMR effect near the first magnetic transition temperature in the $A_{14}MnPn_{11}$ family has already been discussed in previous studies.[35,39−41] The behavior is generally associated with a transition from a low-temperature metallic ferromagnetic phase to a high-temperature semiconducting paramagnetic phase which occurs at or near T_C. As was observed in other classes of CMR compounds,[42−44] conduction electrons will experience less spin scattering from the long-range magnetic ordering, which is induced by a magnetic field, and subsequently the resistivity of the compound decreases. But the CMR effect in the $A_{14}MnPn_{11}$ compounds cannot be attributed to any of the previous mechanisms proposed for other CMR compounds. For the perovskites, enhanced carrier hopping between the heterovalent Mn ions with mutually aligned spins is thought to be related to the metallic ferromagnetic state,[45] and for the pyrochlores, s−d scattering between a low density of conduc-

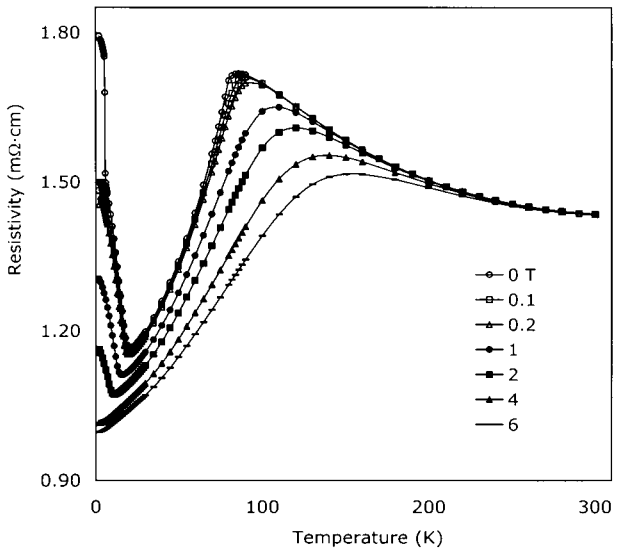

Figure 10. Magnetoresistance of $Eu_{13}CaMnSb_{11}$ single crystal with *c*-axis parallel to the applied field.

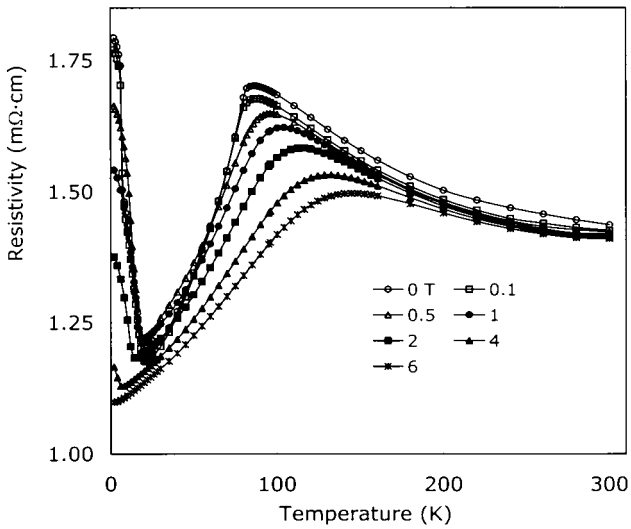

Figure 11. Magnetoresistance of $Eu_{13}CaMnSb_{11}$ single crystal with *c*-axis perpendicular to the applied field.

(38) Ramirez, A. P. *J. Phys.: Condens. Matter* **1997**, *9*, 8171.
(39) Chan, J. Y.; Kauzlarich, S. M.; Klavins, P.; Liu, J.-Z.; Shelton, R. N.; Webb, D. J. *Phys. Rev. B* **2000**, *61*, 459−463.
(40) Chan, J. Y.; Kauzlarich, S. M.; Klavins, P.; Shelton, R. N.; Webb, D. J. *Phys. Rev. B* **1998**, *57*, R8103−R8106.
(41) Webb, D. J.; Cohen, R.; Klavins, P.; Shelton, R. N.; Chan, J. Y.; Kauzlarich, S. M. *J. Appl. Phys.* **1998**, *83*, 7192−7194.
(42) von Helmolt, R.; Wecker, J.; Holzapfel, B.; Schultz, L. *Phys. Rev. Lett.* **1993**, *71*, 2331.
(43) Subramanian, M. A.; Toby, B. H.; Ramirez, A. P.; Marshall, W. J.; Sleight, A. W.; Kwei, G. H. *Science* **1996**, *273*, 81.
(44) Ramirez, A. P.; Cava, R. J.; Krajewski, J. *Nature* **1997**, *386*, 156.

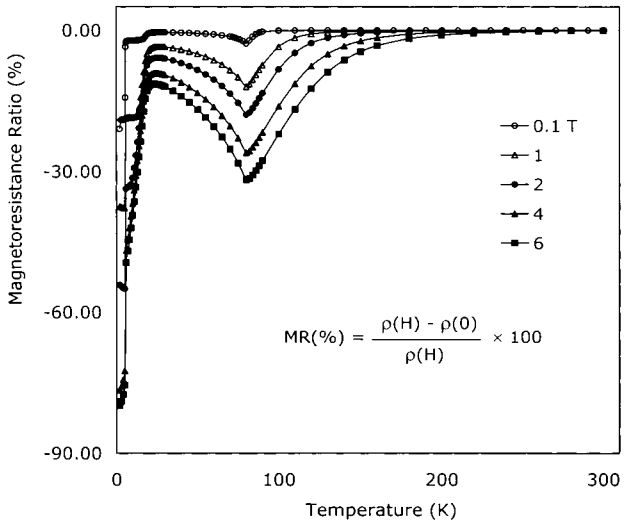

Figure 12. Magnetoresistance ratio vs temperature of $Eu_{13}CaMnSb_{11}$ single crystal oriented parallel to the applied field.

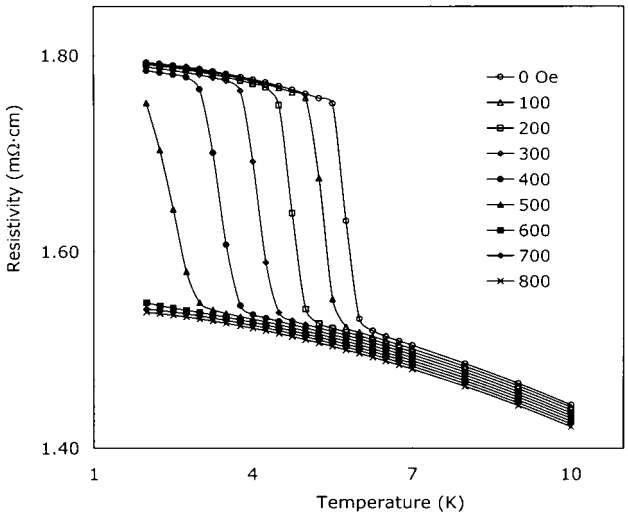

Figure 13. Resistivity vs temperature below the critical field of $Eu_{13}CaMnSb_{11}$ single crystal with *c*-axis parallel to the applied field.

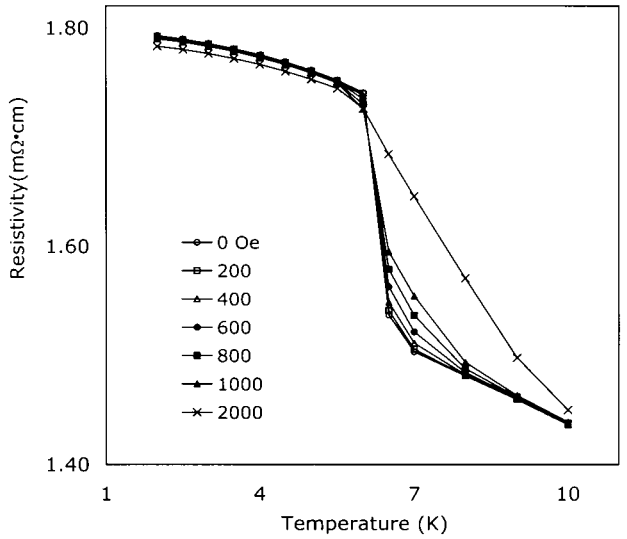

Figure 14. Resistivity vs temperature below the critical field of $Eu_{13}CaMnSb_{11}$ single crystal with *c*-axis perpendicular to the applied field.

tion electrons and the local Mn spins, which originate from different lattice sites, is responsible for the CMR effect of the compounds.[46] In the $A_{14}MnPn_{11}$ compounds, it has been suggested that s−d interactions based on the RKKY-type exchange cause the CMR effect and both the magnetism and resistivity originate from the same dilute Mn spins in the compound.

The consistency between the paramagnetic Curie constant and a peak point in the resistivity curve found in this study also indicate that the metallic state of the $A_{14}MnPn_{11}$ compound is closely related to the ferromagnetic ordering of Mn−Mn which is reinforced by the Mn−Eu exchange interactions. Experimental data show the importance of Mn in the electrical transport of the $A_{14}MnPn_{11}$ compounds. When the transition metal is replaced by a main group element, for example, $Eu_{14}GaSb_{11}$, the peak around 90 K in the resistivity disappears, accompanied by the loss of long-range magnetic ordering in the magnetization curve.[47] Thus, the Mn 3d contribution is believed to be the dominant effect rather than the Eu 4f at the Fermi level even in this dilute Mn system. This generalization would be applicable also in a band structure theory of 3d−4f compounds.[6] The 3d band is much narrower than the 5d band, whose states are almost unoccupied in the lanthanides, and the 4f states are treated as spatially localized "open (shell) cores (states)" and not hybridizing with the valence states. As a consequence, the rare earth 4f states do not contribute to chemical bonding and the large atomic 4f moments would be regarded as localized spin scatterers which would have influence on the magnetic polarons of the compound.

The general behavior in the transport properties of $Eu_{13}CaMnSb_{11}$ is the same as that for $Eu_{14}MnSb_{11}$. The effect of Ca substitution for Eu does not have a strong influence on the electronic conduction except for the shifts in the transition temperatures as shown in Figures 10 and 11, indicating little contribution of Eu 4f states to the transport properties of the compound. The first decrease of resistivity below the Curie temperature is attributed to a canted-type magnetic ordering of Mn and Eu ions, and the next resistivity increase, below 24 K, is due to the onset of antiferromagnetic ordering of Eu−Eu in the compound. The close relation between magnetic and electronic properties suggests significant spin scattering by magnetic ions. Thus, we propose again that the MR effect in the compound could be explained by the s−d exchange interaction between conduction electrons mainly composed of Mn s electrons and magnetic ions from Mn d and Eu f electrons.

Low-Temperature Magnetism and Resistivity. We now turn to the very low temperature magnetic transition at 6 K. Figures 13 and 14 present resistivity plots, below 10 K, which were measured along the crystal *c*-axis aligned parallel and perpendicular to the applied magnetic field, respectively. This transition has not been observed in previous studies of $Eu_{14}MnSb_{11}$ since a detailed magnetization measurement at the low

(45) Millis, A. J.; Shraiman, B. I.; Mueller, R. *Phys. Rev. Lett.* **1996**, *77*, 175.
(46) Ramirez, A. P.; Subramanian, M. A. *Science* **1997**, *277*, 546−549.
(47) Kim, H.; Kauzlarich, S. M. In preparation.

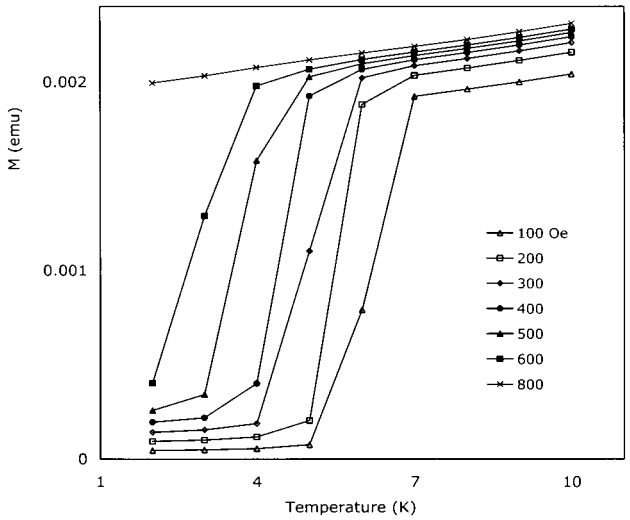

Figure 15. Temperature-dependent magnetization below the critical field of $Eu_{13}CaMnSb_{11}$ single crystal with *c*-axis parallel to the applied field.

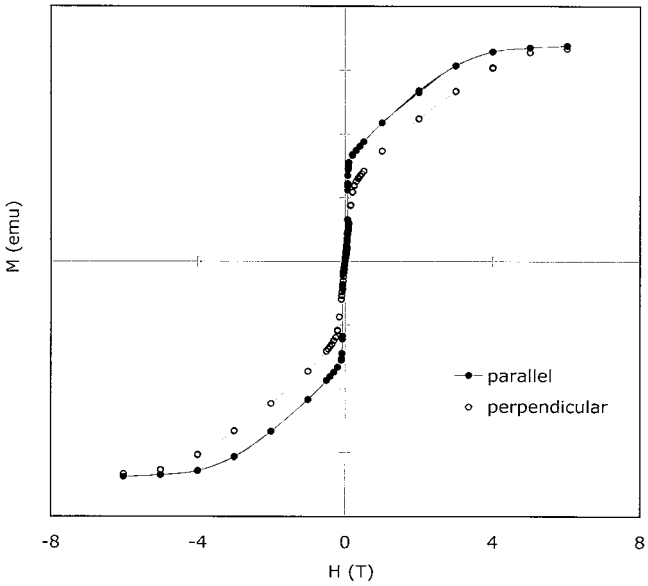

Figure 16. Field-dependent magnetization of $Eu_{13}CaMnSb_{11}$ single crystal with *c*-axis oriented parallel and perpendicular to the applied magnetic field at 2 K.

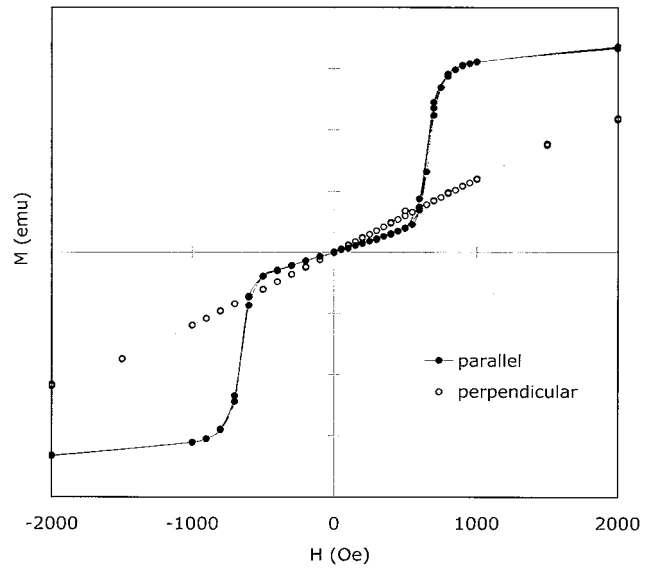

Figure 17. Field-dependent magnetization of $Eu_{13}CaMnSb_{11}$ single crystal around the critical field at 2 K.

temperature, below 5 K, had not been performed. A similar transition was first observed in $Eu_{13.97}Gd_{0.3}MnSb_{11}$ and has been found in this solid solution study. The low-temperature magnetization of a single crystal of $Eu_{13}CaMnSb_{11}$ in low fields is presented in Figure 15. In Figure 13, a sudden jump in resistivity is present at 6 K in zero field and the transition temperature is suppressed as increasing field is applied. The increase in resistivity can be directly related to the onset of a new magnetic transition in Figure 15. Magnetization of the crystal sample suddenly drops at 6 K in a 100 Oe applied field, and the transition is suppressed by applying higher fields. When the crystal is placed perpendicular to the applied field, the magnetic field dependence of the resistivity is somewhat different. The transition is not shifted to lower temperatures and the slope of the increase changes slightly as higher fields are applied (Figure 14). This is a unique example which shows that the magnetocrystalline anisotropy influences the electronic conduction of the compound. By the placement of a crystal with a different orientation in a magnetic field, the electrical properties of the material are affected.

To study the details of this transition, field-dependent magnetization of a single crystal of $Eu_{13}CaMnSb_{11}$ has been measured and plotted in Figure 16. The two different directional magnetizations approach the same saturation value by different pathways. The final magnetic phase of the compound, in applied fields above 5 T at low temperatures, will be ferromagnetic for both directions but have different magnetization processes due to magnetocrystalline anisotropy which results mainly from the Eu 4f sublattices. At very low fields, below 600 Oe, there is another antiferromagnetic phase in the parallel direction. One can see a typical metamagnetic behavior in the parallel direction as shown in Figure 17. It is stable only at low temperatures and low fields and is strongly related to the crystal direction. The spin reorientation of 4f electrons may occur at elevated fields or elevated temperatures since their spin is more temperature and field dependent than 3d electrons.

Summary

In summary, the electronic structure and magnetism of the $Eu_{14}MnPn_{11}$ compounds can be understood by general consideration of the 3d−4f compounds, categorized as the RTX compounds (R = rare earths, T = transition metals, X = main group 13−15 elements). The itinerant Mn 3d states participate in metallic conduction, and their spin polarization is the driving force for the magnetic order in these compounds. The localized Eu 4f states form magnetic subsystems from the interatomic 3d−5d coupling, mediated by intraatomic 4f−5d interactions, and interatomic 4f−4f exchange interactions. Their contribution to electronic conduction would be limited due to the localized character of the 4f states. The ferrimagnetic spin arrangement or canted configurations between magnetic sublattices are observed. This study shows that preferential replacement of Eu(3) and/or Eu(1) sites by Ca raises the

T_C and suppresses the low-temperature antiferromagnetic ordering. This implies that Eu(3) and/or Eu(1) sites contribute to frustration in the system and loss of frustration occurs upon substitution of the nonmagnetic Ca ion.

Resistivity of the compound shows a close connection to the spin polarization of the metal ion constituents and can be successfully explained on the basis of s−d spin scattering between conduction electrons and magnetic ions. Small amounts of nonmagnetic Ca substitution onto the Eu sites reveal the detailed crystallographic environments of each site preference and confirm the localized character of Eu 4f states.

Acknowledgment. We thank the National Science Foundation (DMR 9803074) for funding. We thank R. N. Shelton for use of the SQUID magnetometer. The Bruker SMART 1000 diffractometer was funded in part by NSF Instrumentation grant CHE-9808259.

Supporting Information Available: Tables of crystal data, atomic coordinates, bond distances, and anisostropic displacement parameters (PDF). X-ray crystallographic data in CIF format. This material is available free of charge via the Internet at http://pubs.acs.org.

CM010512S